Condition Assessment of a Metallic Runway Beam Based on Dynamic and Static Testing

Check for updates

Diogo Ribeiro ⬛, **Cristina Alves Ribeiro** ⬛, **Jorge Leite** ⬛,
Cássio Bragança ⬛, **Manuel Silva, Nuno Pinto** ⬛, **Pedro Conceição,**
and António Gaspar

Abstract This work describes the experimental evaluation of the structural condition of a metallic runway beam located in a heavy industry facility. The study involved carrying out an ambient vibration test, aiming the identification of the modal parameters of the beam, in addition to a static test under the action of a transportation vehicle carrying heavy raw material. The static test was mainly focused on the measurement of deformations and displacements on critical sections of the beam. The results of both tests will be useful for the experimental calibration of the numerical model of the beam developed by the designers, which will provide support for the structural rehabilitation and strengthening of the runway beam.

Keywords Structural condition assessment · Runway beam · Ambient vibration test · Static tests · Transportation vehicle

D. Ribeiro (✉) · J. Leite
CONSTRUCT-LESE, Polytechnic of Porto—School of Engineering, Porto, Portugal
e-mail: drr@isep.ipp.pt

C. A. Ribeiro
Senqual, Vila Nova de Gaia, Portugal

C. Bragança
Department of Structural and Geotechnical Engineering, Polytechnic School at the University of São Paulo, São Paulo, Brazil

M. Silva
Polytechnic of Porto—School of Engineering, Porto, Portugal

N. Pinto
CONSTRUCT-LESE, University of Porto—Faculty of Engineering, Porto, Portugal

P. Conceição · A. Gaspar
IDOM Engenharia—Serviços de Engenharia e Consultoria, Lda., Lisbon, Portugal

1   Introduction

The increasing environmental concerns and the restricted budget of many infrastructure managers has been led to an increasingly reuse of existing metallic structures. In most cases, this reuse involves some type of structural rehabilitation/strengthening to prepare the structure for more severe loading and environmental conditions. To guarantee the success of these strengthening operations, recent studies [1–3] stand out the need to have a deep knowledge about the current structural integrity conditions for the optimal design of strengthening solutions and, afterwards, evaluate their effectiveness.

Mirza et al. [4] studied the effectiveness of retrofit techniques in increasing the fatigue life of railway bridge beams. To guide the retrofit actions, numerical and experimental studies were carried out on a beam from an old bridge, with 120 years of use, and a new one. Based on these studies, cracks were introduced in the numerical model in critical locations, and, in the areas affected by the stress concentration of the crack, structural strengthening actions were proposed. These actions proved to be quite effective in smoothing the stress field in the critical region as well as extending the fatigue life of the beam. Another important finding of the study was the lower strength capacity of the old beam when compared to the numerical predictions. This was attributed to the existence of damage, which was increasingly accumulated during its use, and was not properly defined in the numerical simulation.

Due to these uncertainties regarding the integrity of an existing structure as well as the imprecisions in modeling some complex structural behaviors, most of authors [1, 5–7] use numerical models calibrated with experimental data to plan, execute and evaluate the performance of strengthening structural interventions.

Based on calibrated numerical models, Ghorbanzadeh et al. [5] conducted a parametric study to find optimal geometries for structural details intended to strengthen beam-column joints in metallic structures. Based on these studies the authors proposed an optimized solution to reinforce existing pinned steel connections. Results indicated a significant increase in the tensile resistance and rotation capacity of the joint, increasing its robustness to prevent progressive collapse of a building under extreme loading scenarios, as well as accomplishing the design standards requirements.

Rodrigues et al. [1] proposed a strain monitoring system based 80 fiber optic sensors to monitor all stages of the structural rehabilitation of a historic railway bridge. The monitoring system, with the support of a calibrated numerical model, proved to be crucial for understanding the structural behavior of the bridge and planning the stages of replacement of the damaged elements. Once the rehabilitation works were completed, the monitoring system allowed the evaluation of the effectiveness of the strengthening strategies, as well as the calibration of an updated numerical model of the bridge, to serve as a basis for further interventions during life cycle.

Given the importance of properly characterizing the structural behavior for rehabilitation interventions, this work presents the stages of an experimental condition

assessment of a metallic runway beam. The runway beam is part of an overhead crane designed to transport very high loadings inside a large-scale industrial facility. The structural behavior of the beam was evaluated based on two types of tests. First, an ambient vibration test was performed to estimate the natural frequencies, damping coefficients and modes of vibration resorting to dedicated modal identification techniques. Second, the deformations and displacements were monitored at several points of the beam during the bridge crane operation transporting heavy loads. The data and conclusions derived from these tests will better guide the designers in the elaboration of optimal solutions for the structural strengthening.

2   The Metallic Runway Beam

The runway beam under study (RWB7) is connected to an identical neighboring beam (RWB9). Both beams are simply supported on metallic pillars and have a span length of 15.0 m (Fig. 1a). The connection between RWB7 and RWB9 is performed by bracings disposed in the form of a plane truss on the horizontal plane, which is connected to the top flanges of the main beams. A transport vehicle, which is part of an overhead crane, runs on the RWB7 beam moving heavy raw material through an industrial facility.

The cross section of the beams (Fig. 1b) is a welded I profile with a height of 1820 mm and a width of 450 mm. The thickness of the web plates and the flanges is equal to 20 mm and 30 mm, respectively. On the outer face of both flanges there are reinforcement plates. These reinforcement plates are 550 mm wide, 30 mm thick and welded to the flanges at their ends. The runway beam includes an A100 type rail attached to the upper face of the reinforcement plate by proper fixing devices. In Fig. 1b the typical cross-sections of the runway beam and rail are presented, as well as the rail fixing devices.

3   Ambient Vibration Test

The ambient vibration test of the runway beam aimed to estimate the natural frequencies, damping coefficients and mode shapes in the vertical and transversal directions.

3.1   Experimental Setup

Figure 2 depicts the measurement positions used during the ambient vibration test. A testing technique based on fixed reference points (marked in red in Fig. 2) and mobile points (marked in yellow in Fig. 2) was adopted. The response was evaluated
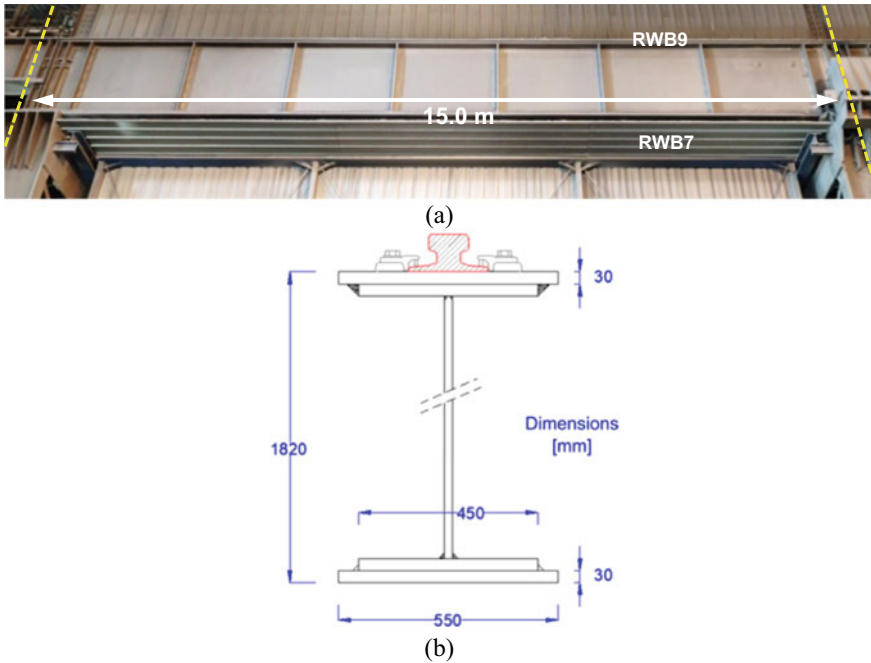
Fig. 1 Runway beams: **a** overview and **b** cross section of RWB7 beam

in terms of accelerations in a total of 20 measurement points. Points 1–8 and points 13–20 were located on the lower flange of beams RWB7 and RWB9, respectively, and points 9–12 were located on the upper flange of beam RWB7. The points were disposed in a regular mesh to facilitate the visualization of the mode shapes.

In total 10 high-sensitivity piezoelectric accelerometers PCB model 393B12, with a measurement range of ± 0.5 g, a sensitivity equal to 10 V/g and a frequency range of 0.15–1000 Hz, were used during the tests. The accelerometers were fixed to the runway beam trough welded angles as presented on the details of Fig. 2. Since only 10 accelerometers were available, the test was conducted in four different experimental setups keeping the reference accelerometers in the same position.

The data acquisition was performed by means of a NI cDAQ-9178 system using three modules NI 9234 for IEPE-type accelerometers with a resolution of 24 bits. The time series were acquired over periods of 8 min with a sampling frequency of 2048 Hz, posteriorly decimated to a frequency of 256 Hz.
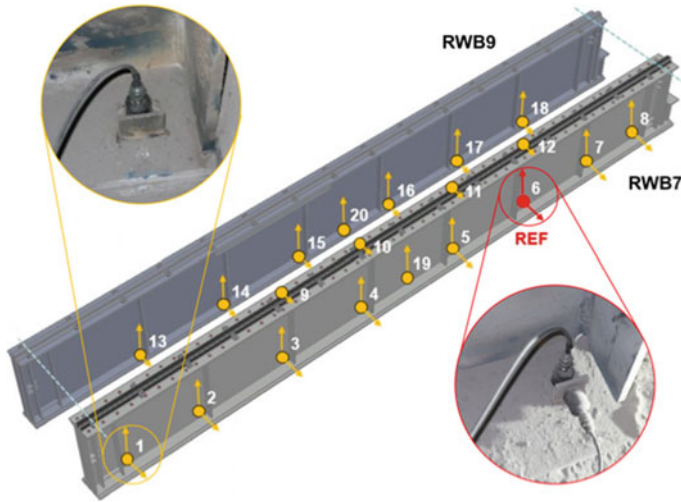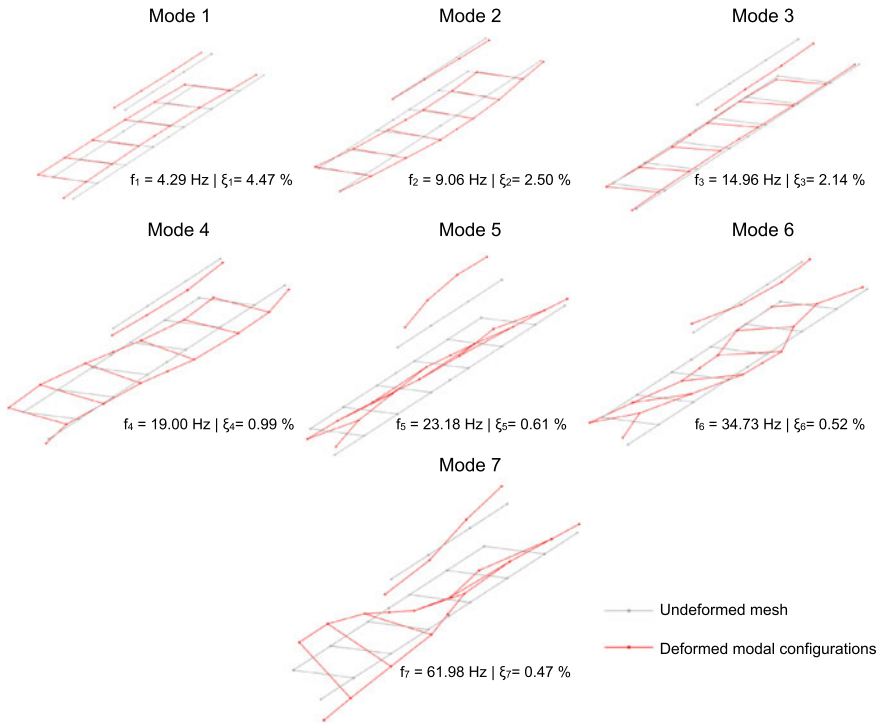
Fig. 2 Ambient vibration test: fixed (red) and mobile (yellow) accelerometers positions

3.2 Modal Identification

The identification of modal parameters was performed by applying the Enhanced Frequency Domain Decomposition method (EFDD). The average and normalized singular values of the spectra matrix of all experimental setups, obtained by applying the EFDD method, are presented in Fig. 3. The identification of the most relevant natural frequencies was performed by evaluating the abscissa in correspondence with the peaks of the curve of the first singular value. In the Fig. 3 the peaks corresponding to the 7 identified vibration modes of the runway beam, whose natural frequencies are ranged between 4.29 and 61.98 Hz, are highlighted by red circles.
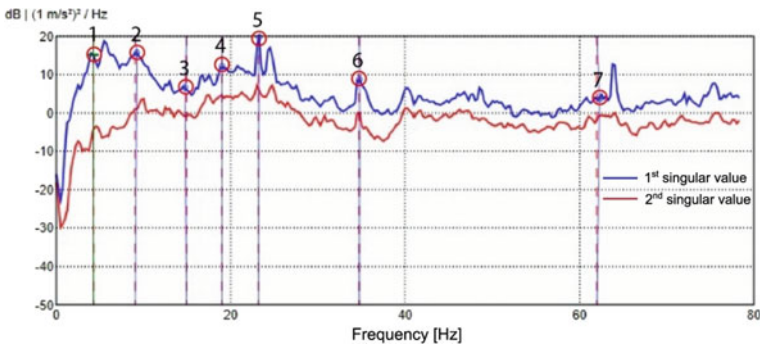
Fig. 3 EFDD method—average and normalized singular values of the spectral density matrices and identified operational modes

Mode 1   Mode 2   Mode 3

$f_1 = 4.29$ Hz | $\xi_1 = 4.47$ % $f_2 = 9.06$ Hz | $\xi_2 = 2.50$ % $f_3 = 14.96$ Hz | $\xi_3 = 2.14$ %

Mode 4   Mode 5   Mode 6

$f_4 = 19.00$ Hz | $\xi_4 = 0.99$ % $f_5 = 23.18$ Hz | $\xi_5 = 0.61$ % $f_6 = 34.73$ Hz | $\xi_6 = 0.52$ %

Mode 7

— Undeformed mesh

— Deformed modal configurations

$f_7 = 61.98$ Hz | $\xi_7 = 0.47$ %

Fig. 4 Modal configurations for 1st to 7th modes (undeformed/deformed shapes) and indication of derived experimental modal parameters

The modal configurations, natural frequencies and damping coefficients associated with each of the 7 identified modes are presented in Fig. 4 based on a perspective view.

The analysis of modal configurations allows to identify modes associated with bending/torsion movements of beams and support columns with very good definition. Mode 1 is possibly associated with the bending movement of the support pillars in the transverse direction, which can be indirectly confirmed by the rigid body translation movement of the beam. Mode 2 is associated with the transverse bending movement of the lower flanges of both beams, with negligible vertical movements and practically no transverse movements at the supports. It is interesting to notice the absence of movements of the upper flange of RWB7 beam. In mode 3 transverse and differential bending movements occur between the upper and lower flanges of the beams with no significant vertical movements. Mode 4 is associated with the second transverse bending movement of the lower flanges of both beams. Once again, the upper flange of RWB7 has a negligible movement in the transverse direction. Mode 5 refers to the out-of-phase first vertical bending mode of each of the beams. This out-of-phase bending causes a global torsion effect, since when one beam goes up the other goes down and vice versa. In this mode the beam also presents some transversal

displacements that cannot be neglected. Mode 6 is related to the 3rd transverse bending movement of the lower flanges of both beams. The movements of the upper flange in the transverse direction appear to be synchronous with the movements of the lower chords. In this case the beam also shows some vertical displacements that cannot be neglected. Finally, mode 7 refers to the second vertical bending movement of each of the beams. The modal configuration is anti-symmetrical and formed by two semi-waves. Like in mode 5, the movements of both beams are out-of-phase, resulting in a non-uniform global torsion effect. Regarding the modal damping coefficients, all values remained between 0.47 and 4.47%, and a reduction of the damping values occur with the increase of the natural frequency.

4   Static Tests Under Operational Live Loads

In this section, the details and results of the static tests conducted under the action of a heavy loading from the transport vehicle are presented. These tests aim a better understanding of the structural behavior of the runway beam under the loading schemes to which is normally subjected. During the tests were performed the measurement of deformations, displacements, and temperatures in various sections of the RWB7 beam.

4.1   Experimental Setup

This subsection describes the instrumentation installed on the runway beam for measuring the displacements and deformations during the operation of the transportation vehicle carrying heavy raw material at high temperatures. The instrumentation was divided into two groups: (i) transducers for measuring deformations and temperatures, and (ii) transducers for measuring displacements.

Strain and Temperature Measurements. The strain measurement system involved the installation of 14 electrical resistance strain gauges in critical locations of the beam. This system also included two thermos-resistors for measuring the temperatures on the beam surface. Figure 5 presents the positioning scheme adopted for the 14 strain gauges (E1 to E14) and the two temperature sensors (TR1 and TR2). All the strain gauges were weldable encapsulated sensors, model LS31HT-6/350VE from HBM, with pre-installed wires, self-compensated for the effect of temperature and with a nominal resistance equal to $350 \, \Omega \pm 0.4\%$. This strain gauge model was selected due to its high resistance to aggressive environments with high temperatures, being compatible with the industrial conditions in which the test was conducted. The connection of the strain gauges to the acquisition system was carried out in a three-wire 1/4 Wheatstone bridge circuit. The thermos-resistors are RS-Pro weldable sensors, model Pt 100, and are connected to the data acquisition by 2 wires.
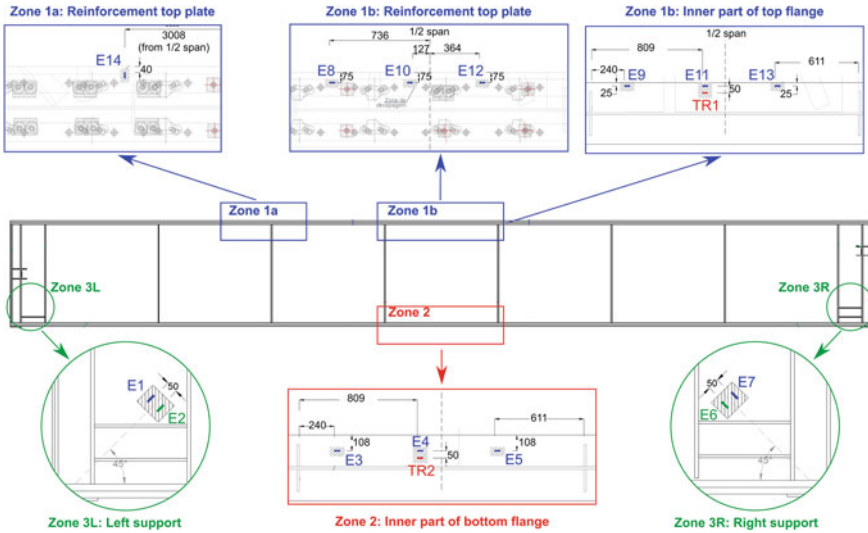
Fig. 5 Location zones of strain gauges (E1 to E14) and thermos-resistors on (TR1 and TR2) the runway beam. Dimensions in (mm)

Displacement Measurement. The displacement measurement system involved measuring the vertical displacements of the runway beam, as well as measuring the relative vertical displacement between the upper flange reinforcement plate and its top flange. This last measurement intended to track a possible gap between these two components. The measurement of the vertical displacements of the beam was performed using a precision topographic system based on a Leica TCRM 1203 total station and topographic reflective targets (prisms type) fixed to the beam in 7 individual positions depicted in Fig. 6 (T1 to T7). The measurement technique is based on optical principles and ensures measurement errors on the vertical displacements less than ±1 mm. The relative displacement measurement involved the installation of a spring-type LVDT, model DCTH 1000A from RDP. The LVDT was fixed to the beam's web by means of a welded plate and clamps, and the extremity of the external shaft was in direct contact with the under face of the reinforcing top plate (Fig. 6). Therefore, a punctual drilling of the upper flange of the beam was carried out, as detailed in Fig. 6.

Data Acquisition System. The data acquisition of the static tests under operational loads was performed by means of a NI cDAQ-9188 system and using NI 9236 modules for signal conditioning of strain gauges, NI 9217 modules for conditioning the thermo-resistance signal and NI 9239 modules for conditioning the LVDT signal.
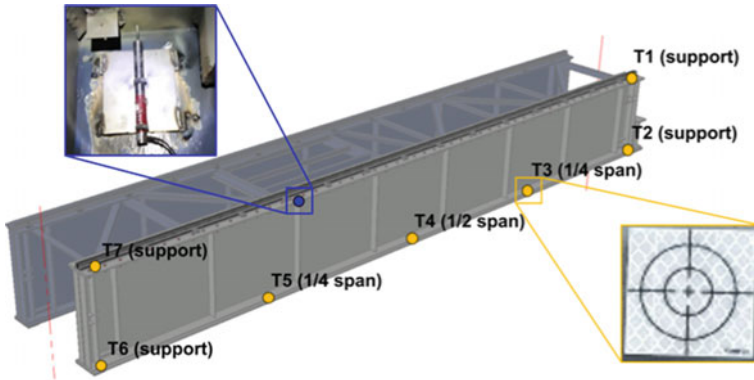
Fig. 6 Displacement measurement setup: Indication of the positioning of topographic targets (T1 to T7) and LVDT

4.2 Loading Strategy

The loading strategy consisted of positioning the heavy load transport vehicle in two different positions. The first position (Fig. 7a) is the one that resulted in the highest shear force value (V_{max}). The second position (Fig. 7b) induces the highest bending moment value (M_{max}). Both positions were estimated with the support of a numerical model. A schematic representation of the crane over the beam in the positions of V_{max} and M_{max} is presented in Fig. 7.
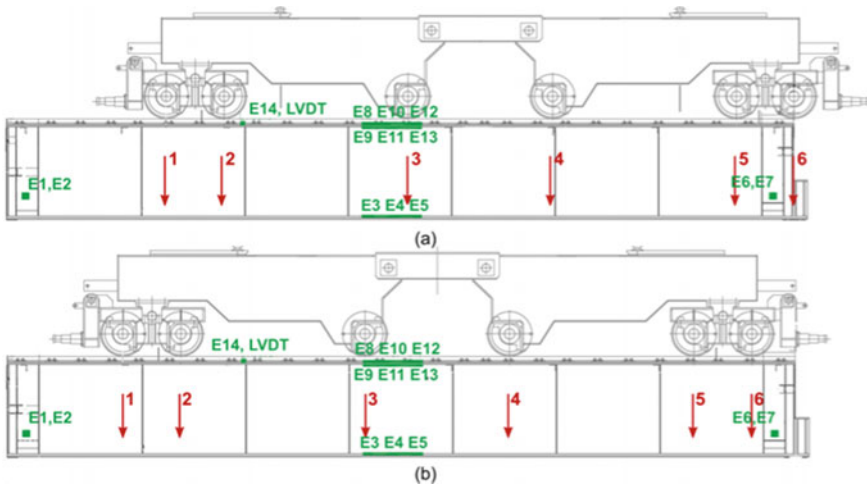
Fig. 7 Positions of the bridge crane wheels, of extensometers E1 to E14 and of the LVDT on the runway beam for the maximum values of: **a** shear force (V_{max}), and **b** bending moment (M_{max})

The exact position of the bridge crane wheels is aligned or very close to some sensors' positions. For example, in the positioning of the bridge crane for V_{max}, it is visible that wheel 3 is on the alignment of the strain gauges E12/E13/E5, while in the positioning for M_{max}, the same wheel is on the alignment of the strain gauges E8/E9/E3. In case of V_{max} positioning, there is also a proximity of the wheel 2 to the strain gauge E14 and to the LVDT.

## *4.3   Results and Analysis*

Figure 8 presents the stress records (derived from the deformations), the relative displacements between the reinforcing top plate and the upper flange of the beam and the temperature for the V_{max} and M_{max} positions. In the time histories the V_{max} position was reached approximately at 16:11, while the M_{max} position was reached approximately at 16:14.

Based on the results it is possible to observe that the stress values in the strain gauge pairs E9/E3, E11/E4 and E13/E5 are quite similar, however, with compressive stresses on the upper flange and tension stresses on the lower flange. This was expectable since the sensors are installed at approximately the same distance from the geometric center of the I profile.

On the other hand, the stress values recorded on the upper face of the reinforcing top plate (E8, E10 and E12) do not follow the assumption of a linear variation of stresses in the section. The stresses recorded at these locations seem to be closely dependent on the position of the wheels, i.e., on the fact that the wheels positions are (or not) close to the section where the sensor is installed. This finding seems to indicate a relevant local behavior of the reinforcement plate due to a poor transmission of stresses with the upper flange.

The stress values recorded on the strain gauge E14, positioned in the direction transverse to the beam axis, seem to corroborate the fact that there is an important local behavior of the reinforcing plate, since they are highly dependent on the position of the load. As examples, it should be refereed the V_{max} position, where the second wheel (see Fig. 7) is positioned in the vicinity of the strain gauge E14, and the M_{max} position, where there are no wheels close to the strain gauge E14. In the case of V_{max} position, there was a very significant increase in the stresses in the transverse direction, while in the M_{max} position these values are practically null.

Furthermore, the values of the relative displacement between the reinforcement top plate and the upper flange reveal that these plates are not effectively connected. This can be seen by the result regarding the position of V_{max}, for which the 2nd wheel is close to the LVDT section, and there is a visible variation in the relative displacement when the vehicle leaves this position. Once again, this finding confirms the local behavior of the reinforcement plate: it tends to contact with the upper flange in the case of a nearby wheel; or tends to recover and remain a gap with the removal of the wheel. Regarding the temperature levels, it remained almost constant near 45 °C.
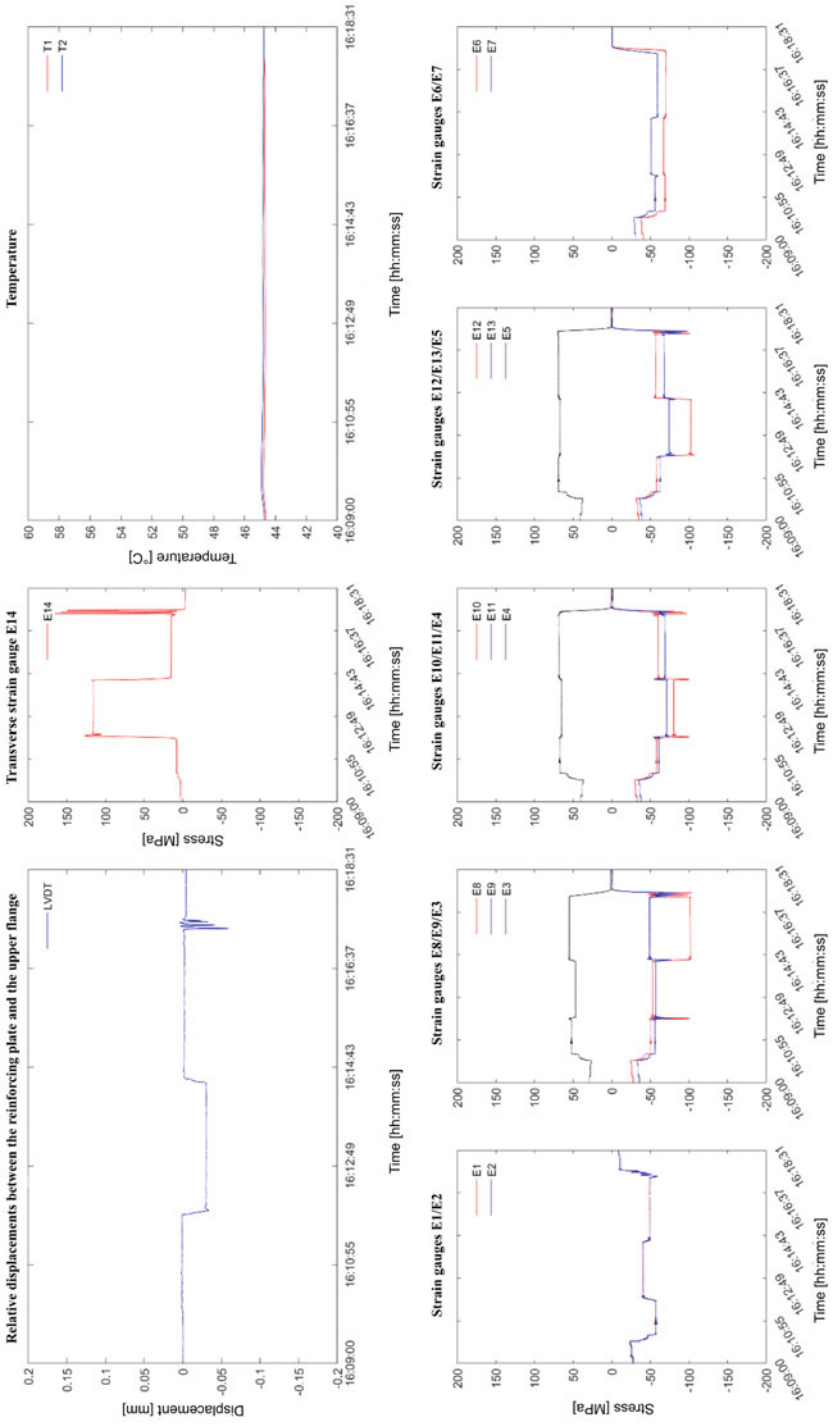
◄**Fig. 8** Measurement results on the static test under operational loads for V_{max} and M_{max} positions: strain gauges, LVDT and temperature sensors
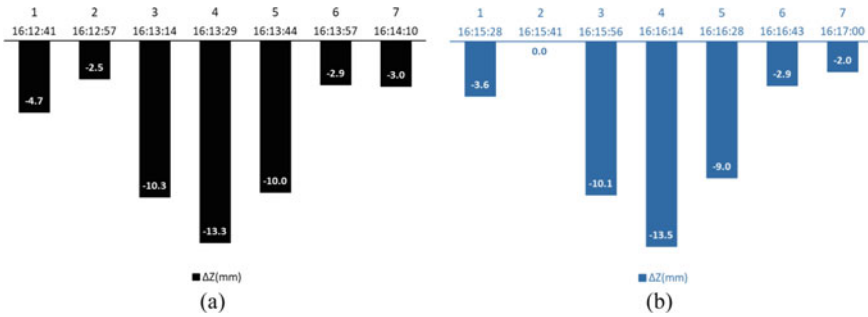
Fig. 9 Measurement of vertical displacements based on a topographical survey for targets T1 to T7: **a** V_{max} position, and **b** M_{max} position

The values of the absolute vertical displacements derived from the topographic survey for the V_{max} and M_{max} positions are presented in Fig. 9a, b respectively. The maximum displacement values were obtained in the ½ span section and are equal to 13.3 mm/13.5 mm for V_{max} and M_{max} positions, respectively. The results also evidence a consistent deformed configuration of the beam, which is virtually visible by sequentially analyzing the displacements between positions of targets T2 to T6. Non-zero vertical displacements were also recorded in both supports (targets T1/T2 and T6/T7) and with values of the same magnitude in most situations.

5   Conclusions

In this work, the results of the experimental condition assessment of a metallic runway beam were presented. The study included two phases, an ambient vibration test and a static test under operational live loads.

The ambient vibration test was intended to characterize the natural frequencies, damping coefficients and modal configurations of the RWB7 beam in the transverse and vertical directions. The application of the EFDD method to the experimental records allowed the identification of 7 global vibration modes with frequencies ranged between 4.29 and 61.98 Hz and referring to bending/torsion modes with very good definition.

The static test under operational live loads involved the measurement of strains, temperatures, and displacements in different parts of the RWB7 beam, as well as the relative displacement between the reinforcement top plate and the upper flange. Additionally, the absolute vertical displacements of the runway beam were measured with the support of a precision topographic survey. The results led to conclude that the

reinforcement top plate was not properly connected to the beam upper flange. This finding was proven due to the non-linear distribution of the stresses along the beam cross section and particularly at the level of the reinforcement top plate. Additionally, it was possible to observe an important local structural behavior strongly dependent on the position of the loads, as stated by the transverse stresses in the reinforcement top plate and in the relative displacements measured between the reinforcement top plate and the upper flange.

In future developments, the calibration of a numerical model of the runway beam will be performed based on the results of the ambient vibration test, as well as the results of the static tests under operational live loads. The model calibration strategy will involve an iterative methodology based on genetic algorithms [8, 9]. The updated models will give an important contribute for the designers in achieving optimized strengthening solutions, and consequently, an extension of the beam life cycle.

References

1. Rodrigues, C., Cavadas, F., Félix, C., Figueiras, J.: FBG based strain monitoring in the rehabilitation of a centenary metallic bridge. Eng. Struct. **44**, 281–290 (2012). https://doi.org/10.1016/j.engstruct.2012.05.040
2. Xie, Q., Zhang, J.: Experimental study on failure modes and retrofitting method of latticed transmission tower. Eng. Struct. **226**, 111365 (2021). https://doi.org/10.1016/j.engstruct.2020.111365
3. Chen, X., Ding, M., Zhang, X., et al.: Experimental investigation on seismic retrofit of gravity railway bridge pier with CFRP and steel materials. Constr. Build. Mater. **182**, 371–384 (2018). https://doi.org/10.1016/j.conbuildmat.2018.06.102
4. Mirza, O., Shill, S.K., Mashiri, F., Schroot, D.: Behaviour of retrofitted steel structures using cost effective retrofitting techniques. J. Constr. Steel Res. **131**, 38–50 (2017). https://doi.org/10.1016/j.jcsr.2016.12.026
5. Ghorbanzadeh, B., Bregoli, G., Vasdravellis, G., Karavasilis, T.L.: Pilot experimental and numerical studies on a novel retrofit scheme for steel joints against progressive collapse. Eng. Struct. **200**, 109667 (2019). https://doi.org/10.1016/j.engstruct.2019.109667
6. Sangiorgio, V., Nettis, A., Uva, G., et al.: Analytical fault tree and diagnostic aids for the preservation of historical steel truss bridges. Eng. Fail. Anal. **133**, 105996 (2022). https://doi.org/10.1016/j.engfailanal.2021.105996
7. Clementi, F., Pierdicca, A., Formisano, A., et al.: Numerical model upgrading of a historical masonry building damaged during the 2016 Italian earthquakes: the case study of the Podestà palace in Montelupone (Italy). J. Civ. Struct. Health Monit. **7**, 703–717 (2017). https://doi.org/10.1007/s13349-017-0253-4
8. Alves, V.N., de Oliveira, M.M., Ribeiro, D., et al.: Model-based damage identification of railway bridges using genetic algorithms. Eng. Fail. Anal. **118**, 104845 (2020). https://doi.org/10.1016/j.engfailanal.2020.104845
9. Costa, C., Ribeiro, D., Jorge, P., et al.: Calibration of the numerical model of a short-span masonry railway bridge based on experimental modal parameters. Procedia Eng. **114**, 846–853 (2015). https://doi.org/10.1016/j.proeng.2015.08.038